Combination of Chemical Genetics and Phosphoproteomics for Kinase Signaling Analysis Enables Confident Identification of Cellular Downstream Targets*⑤

Felix S. Oppermann‡§¶, Kathrin Grundner-Culemann‡§¶, Chanchal Kumar‖**,
Oliver J. Gruss‡‡, Prasad V. Jallepalli§§¶¶, and Henrik Daub‡¶‖‖‖

Delineation of phosphorylation-based signaling networks requires reliable data about the underlying cellular kinase-substrate interactions. We report a chemical genetics and quantitative phosphoproteomics approach that encompasses cellular kinase activation in combination with comparative replicate mass spectrometry analyses of cells expressing either inhibitor-sensitive or resistant kinase variant. We applied this workflow to Plk1 (Polo-like kinase 1) in mitotic cells and induced cellular Plk1 activity by wash-out of the bulky kinase inhibitor 3-MB-PP1, which targets a mutant kinase version with an enlarged catalytic pocket while not interfering with wild-type Plk1. We quantified more than 20,000 distinct phosphorylation sites by SILAC, approximately half of which were measured in at least two independent experiments in cells expressing mutant and wild-type Plk1. Based on replicate phosphorylation site quantifications in both mutant and wild-type Plk1 cells, our chemical genetic proteomics concept enabled stringent comparative statistics by significance analysis of microarrays, which unveiled more than 350 cellular downstream targets of Plk1 validated by full concordance of both statistical and experimental data. Our data point to hitherto poorly characterized aspects in Plk1-controlled mitotic progression and provide a largely extended resource for functional studies. We anticipate the described strategies to be of general utility for systematic and confident identification of cellular protein kinase substrates.   *Molecular & Cellular Proteomics 11: 10.1074/mcp.O111.012351, 1–12, 2012.*

Reversible protein phosphorylation by protein kinases represents a key control mechanism in signal transmission and controls nearly all aspects of cellular physiology. Quantitative proteomics approaches that incorporate techniques such as stable isotope labeling by amino acids in cell culture (SILAC),[1] phosphopeptide fractionation and enrichment by strong cation exchange (SCX), and ion metal affinity chromatography (IMAC) together with sensitive high resolution MS analysis and automated peptide identification and quantification have made it possible to monitor phosphorylation-based signaling on a global scale (1–4). Because signaling networks are defined by the underlying kinase-substrate relationships, systematic approaches are required for the comprehensive and confident assignment of cellular kinase substrates (5). To identify cellular substrates, the catalytic activity of a kinase of interest needs to be rapidly regulated to capture a high fraction of direct phosphorylation events. This implies that protein kinase ablation by genetic knockout or RNA interference can be of limited utility, because of secondary changes that can accumulate during the time required for cellular kinase depletion (3, 5). In contrast, pharmacological interference by small molecules allows for rapid modulation of kinase activity and should therefore enable unbiased monitoring of signaling perturbations when combined with advanced MS-based proteomics. Such approaches are ideally based on mono-selective kinase inhibition. Although generally difficult to achieve for naturally occurring kinases, this is considered feasible by chemical genetics using drug-sensitized kinase mutants possessing an enlarged catalytic pocket to accommodate bulky kinase inhibitors (6). Recently, this inhibition strategy has been combined with large scale quantitative phosphoproteomics in efforts to identify cyclin-dependent kinase 1 substrates upon the addition of the purine analog NM-PP1 in yeast cells (7). However, even supposedly selective kinase inhibitors such as the purine analog NM-PP1, which was designed for specific

[1] The abbreviations used are: SILAC, stable isotope labeling by amino acids in cell culture; SCX, strong cation exchange; IMAC, ion metal affinity chromatography; IPI, International Protein Index; FDR, false discovery rate; GO, Gene Ontology; RPE, retinal pigment epithelial; SAM, significance analysis of microarrays; mTOR, mammalian target of rapamycin; EGFR, epidermal growth factor receptor.

inhibition of mutationally sensitized kinase variants, exhibit off-target activity *in vitro* (6–8). Therefore, cellular selectivity control is warranted for confident assignment of kinase-substrate relationships.

Here, our interest was to advance strategies for unbiased and confident identification of cellular downstream targets of protein kinases by using Plk1 (Polo-like kinase 1) signaling in human cells as a model system. Plk1 is a central regulator of cell division with key roles in mitotic entry, bipolar spindle assembly, and chromosome segregation, as well as cytokinesis (9). Consistent with these important functions throughout the M phase, human Plk1 localizes to centrosomes at mitotic entry, then associates with kinetochores, and later accumulates at the central spindle and the midbody in the late M phase (9). Plk1 possesses a carboxyl-terminal Polo box domain involved in the phosphorylation-dependent recruitment of substrate proteins through specific interactions with a Ser-(Ser(P)/Thr(P))-(Pro/Xaa) motif (10).

Plk1 has been analyzed in previous studies to gain further insights into the mechanisms that might execute Plk1 functions in mitosis, including a targeted analysis of selected candidates (11) and a proteomic screening of *in vitro* Plk1-interacting proteins using recombinant Polo box domain as bait (12). Moreover, a recent phosphoproteomics screen reported Plk1 substrate candidates in the mitotic spindle. In this study, phosphorylation changes were measured upon prolonged Plk1 inhibition by either small interference RNA expression or small molecule inhibitor treatment (13). However, none of the previous studies has systematically interrogated the effect of short term Plk1 modulation on a proteome-wide scale in a specificity-controlled manner. Here, we report an advanced concept that implements these criteria for the identification of kinase-regulated phosphoproteins in intact cells. Our goal was to acquire comprehensive and confident data about phosphoregulation of Plk1 downstream targets as proof-of-concept for a tightly controlled approach of general utility for kinase signaling research.

EXPERIMENTAL PROCEDURES

Cell Culture and Treatment—Telomerase-expressing human retinal pigment epithelial (hTERT-RPE) cells in which both genomic *PLK1* loci were disrupted and that expressed either wild-type Plk1 (Plk1^{wt}) or an analog-sensitive Plk1 mutant (C67V/L130G, referred to as Plk1^{as}) as EGFP fusions were used throughout this study (14). For differential SILAC encoding, the cells were grown in a 1:1 mixture of arginine- and lysine-deficient Dulbecco's modified Eagle's medium (Invitrogen) and F12 Ham's medium (Invitrogen) supplemented with L-glutamine (2 mM; PAA Laboratories), sodium pyruvate (1 mM; Invitrogen), 1% penicillin/streptomycin (PAA Laboratories), 10% dialyzed fetal bovine serum (Invitrogen), and either 175 μM unlabeled L-arginine (Arg^0) and 250 μM unlabeled L-lysine (Lys^0) or the same concentrations of L-[U-$^{13}C_6$,$^{14}N_4$]arginine (Arg^{10}) and L-[U-$^{13}C_6$,$^{15}N_2$]lysine (Lys^8) (Sigma). After six cell doublings to ensure complete proteome labeling, 1.6×10^6 cells were seeded per 15-cm dish (in total 12–20 dishes/experiment). 18 h later, 1 μg/ml aphidicoline (Sigma) was added for a further 12 h to synchronize cells in the early S phase. The cells were then washed with PBS and cultured for another 13 h in fresh SILAC medium

containing 50 ng/ml nocodazole (Sigma) and 5 μg/ml 3-MB-PP1 (Priaxon AG, Munich, Germany) to arrest Plk1^{as} or Plk1^{wt} cells in M phase in addition to inhibiting mutant kinase activity in Plk1^{as} cells. The cells were then washed once prior to adding either fresh SILAC medium containing 50 ng/ml nocodazole and 5 μM 3-MB-PP1 to Arg^0/Lys^0-labeled cells or the same medium without 3-MB-PP1 to Arg^{10}/Lys^8-encoded cells for a further 30 min until cell lysis. This labeling scheme was used in two biological replicate experiments with Plk1^{as} (referred to as as1 and as3) and Plk1^{wt} cells (wt1 and wt3), whereas in two further replicate experiments with either cell line reciprocal labeling conditions were used (as2, as4, wt2, and wt4).

Cell Lysis and Immunoblotting—The cells were lysed in 500 μl of 8 M urea, 50 mM Tris-HCl, pH 8.2, 75 mM NaCl, 1 mM EDTA, 1 mM EGTA, 1 mM PMSF, 10 mM NaF, 2.5 mM Na$_3$VO$_4$, 50 ng/ml calyculin A (Alexis Biochemicals), 10 μg/ml aprotinin, 10 μg/ml leupeptin, and 1% phosphatase inhibitor mixture 1 and 2 (v/v) (Sigma) per two 15-cm dishes for 5 min on ice. The cell extracts were sonicated three times for 1 min on ice. Cell debris was then removed by centrifugation, and equal protein amounts from differentially SILAC-encoded cells were pooled for subsequent MS sample preparation. For immunoblot analysis, Plk1^{as} cells were seeded at 180,000 cells/well in 6-well cell culture dishes. The cells were synchronized and treated as in the SILAC experiments with the only modification that the 13-h nocodazole incubation was done both in the presence and the absence of 3-MB-PP1. Lysis was performed with buffer containing 50 mM HEPES-NaOH, pH 7.5, 150 mM NaCl, 0.5% Triton X-100, and all phosphatase and protease inhibitors used for urea lysis of SILAC-encoded cells prior to gel electrophoresis and immunoblotting with monoclonal mouse anti-BubR1 antibody (Cell Signaling Technology, Inc.).

Mass Spectrometry Sample Preparation—Pooled lysates were adjusted to 6 M urea, 1.5 M thiourea and reduced, alkylated, and digested in-solution with endoproteinase Lys-C and trypsin as detailed before (15). Tryptic peptides were then filtered through a 0.22-μm polyvinylidene fluoride membrane (Millipore) and desalted using reversed phase C$_{18}$ SepPak cartridges (500-mg sorbent weight; Waters) as described previously (16). Desalted peptide samples were snap-frozen in liquid nitrogen, lyophilized, and stored at −20 °C. Lyophilized peptides were dissolved in 600 μl of 7 mM KH$_2$PO$_4$, pH 2.65, 30% ACN and loaded onto a 250 × 9.4 mm polySULFOETHYL A column (200 Å pore size and 5-μm particle size; PolyLC) operated with an ÄKTA explorer system (GE Healthcare) at 3 ml/min. The flow-through was collected, and bound peptides were fractionated by a 30-min gradient ranging from 0% to 30% elution buffer (7 mM KH$_2$PO$_4$, pH 2.65, 30% ACN, 350 mM KCl), followed by 10-min washing steps with 100% elution buffer, H$_2$O, and 500 mM NaCl (16). 3-ml fractions were collected throughout SCX separation and pooled based on the measured UV absorption at 215 nm to 12 samples with rather even peptide amounts. After evaporation of ACN, the samples were desalted using reversed phase C$_{18}$ SepPak cartridges (100-mg sorbent weight; Waters) prior to lyophilization.

For phosphopeptide enrichment, lyophilized peptide samples were resuspended in 200 μl of 25 mM formic acid, 40% acetonitrile and incubated with 2.5 μl of PHOS-Select iron affinity gel (Sigma) for 1 h at 25 °C under continuous agitation. Phosphopeptide elution and subsequent desalting with C$_{18}$ StageTips were performed as described (16, 17). StageTip-purified peptide samples were concentrated to 4 μl and mixed with an equal volume of 0.2% TFA, 4% ACN prior to MS analysis of technical replicates of each sample.

Mass Spectrometry Analysis—All of the LC-MS/MS analyses were performed on an linear ion trap (LTQ)-Orbitrap (Thermo Fisher Scientific) connected to a nanoflow HPLC system (Agilent 1100) via a nanoelectrospray ion source (Proxeon Biosystems) as described (2, 15). Briefly, phosphopeptide-enriched samples were resolved by a 15-cm analytical column (75-μm inner diameter) packed with 3-μm

C$_{18}$ beads (Reprosil-AQ Pur; Dr. Maisch, GmbH, Germany) in 140-min runs by a gradient from 5 to 40% acetonitrile in 0.5% acetic acid and at a flow rate of 250 nl/min. Eluting peptides were directly electrosprayed into the mass spectrometer. The LTQ-Orbitrap was operated with Xcalibur 2.0 in the data-dependent mode to automatically switch between full scan MS acquisition in the orbitrap analyzer (resolution $r = 60,000$ at $m/z = 400$) and the acquisition of tandem mass spectra of 10 multiply charged ions by in the LTQ part of the instrument (18). Multi-stage activation was enabled in the linear ion trap to activate neutral loss species of phosphopeptides at 97.97, 48.99, or 32.66 m/z below the precursor ion for 30 ms during fragmentation (19). For all full scans in the orbitrap detector, a lock-mass ion from ambient air (m/z 429.08875) was used for internal calibration as described (2). Typical mass spectrometric conditions were: spray voltage, 2.4 kV; no sheath and auxiliary gas flow; heated capillary temperature, 175 °C; normalized collision energy 35% for multi-stage activation in LTQ. The ion selection threshold was 500 counts for MS/MS. An activation of $q = 0.25$ was used.

Data Processing and Statistical Analysis—All 192 raw files acquired in this study were collectively processed with the MaxQuant software suite (version 1.0.13.12), which performs peak list generation, SILAC-based quantification, estimation of false discovery rates, peptide to protein group assembly, and phosphorylation site localization as described previously (4, 20). Peak lists were searched against a concatenated forward and reversed version of the human International Protein Index (IPI) database version 3.37 (containing 69,141 protein entries and 175 frequently detected contaminants such as porcine trypsin, human keratins, and Lys-C) using the Mascot search engine (Matrix Science; version 2.2.04). Carbamidomethylation of cysteine was set as a fixed modification, and oxidation of methionine, amino-terminal acetylation, losses of ammonia from amino-terminal glutamine and cysteine, and phosphorylation on serine, threonine, and tyrosine were set as variable modifications. SILAC spectra detected by presearch MaxQuant analysis were searched with the additional fixed modifications Arg^{10} and/or Lys^8, whereas spectra for which a SILAC state was not assignable prior to database searching were searched with Arg^{10} and Lys^8 as variable modifications. Accepted mass tolerances were 7 ppm for the MS and to 0.5 Da for MS/MS peaks. The minimum required peptide length was six amino acids, and up to three missed cleavages and three labeled amino acids were allowed. The accepted estimated FDR determined on the basis peptide-spectral matches in the reversed database version was set to 1% for both peptide and protein identifications. Phosphorylation sites were assigned by the post-translational modification scoring algorithm implemented in MaxQuant as described (18, 20).

For phosphorylation site analysis, only those with a localization probability of at least 0.75 (class I sites) were considered. Phosphosite ratios were averaged for each biological replicate experiment in case of SILAC-based quantification in both technical replicate analyses. The resulting quantified phosphosite ratios from biological Plk1^{as} and Plk1^{wt} replicate experiments were considered for all further comparative and statistical analyses. The distribution of phosphosite ratios was visualized by box plots with whiskers indicating five times the interquartile range. Box plots were computed in the R statistical environment (21) and were generated for all individual biological replicate experiments in Plk1^{as} and Plk1^{wt} cells.

For phosphopeptide analysis, all peptide evidences were filtered for a Mascot score of at least 7 and a mass error of less than 5 ppm. Phosphopeptides were specified by their amino acid sequence and number of phosphorylation sites. In each technical replicate experiment, the median SILAC ratio was calculated for repeatedly quantified phosphopeptides. Phosphopeptide SILAC ratios were also averaged for each biological replicate experiment in case such ratios were available for both technical replicates.

To identify differential 3-MB-PP1 phosphoregulation in Plk1^{as} *versus* Plk1^{wt} cells, all phosphosite or phosphopeptide ratios measured in at least two biological replicate analyses of both Plk1^{as} and Plk1^{wt} cells were log$_2$-transformed and subjected to two-class, unpaired significance analysis of microarrays (SAM) analysis (version 3.0, http://www-stat.stanford.edu/~tibs/SAM/sam.pdf) (22). SAM computes a statistics d_i for each ratio to identify significantly different ±3-MB-PP1 ratios in Plk1^{as} *versus* Plk1^{wt} cells and uses permutations of the repeated measurements to calculate false discovery rates (q values) for different values of a threshold parameter Δ. Missing ratio values were imputed by SAM via a K-Nearest Neighbor algorithm normalization (number of neighbors set to 15).

For all regulated phosphosites reported by SAM (up to an FDR of 60%), we further analyzed whether either the Plk1^{as} or the Plk1^{wt} ratio deviated more strongly from one for different Δ parameters. For further bioinformatics analysis, phosphosites and phosphopeptides of the SAM output with a FDR (or q value) of 0% obtained for $\Delta \geq 2.136$ and $\Delta \geq 2.363$, respectively, were considered as regulated.

CK1δ Kinase Assay—*In vitro* CK1δ activity in the presence of different concentrations of 3-MB-PP1 was measured on the substrate CK1tide (200 μM; Upstate Biotechnology Inc.) in buffer containing 8 mM MOPS-NaOH, pH 7.0, 0.2 mM EDTA, 10 mM magnesium acetate, 0.1 μM ATP, 0.5 μCi of [γ-^{33}P]ATP, and different 3-MB-PP1 concentrations. After a 30-min preincubation with inhibitor on ice, kinase reactions were started by ATP addition and performed for 10 min at 30 °C in a final volume of 25 μl. Phosphate incorporation and IC$_{50}$ values were determined as described (23).

Bioinformatics Analysis—Sequence stretches of ±6 residues for all up-regulated serine phosphorylation sites were analyzed by Motif-X to extract significantly overrepresented motifs compared with the background of all SAM-analyzed class I serine sites (24). In Motif-X analysis, the minimum number of occurrences and the required motif significance were set to 10 and 10^{-6}, respectively. Furthermore, sequence windows of all phosphosites were analyzed for the presence of the Plk1 consensus motif (25), a (D/E/N)X(pS/pT) motif, and the Polo box domain recognition motif (10). For each of these three motifs, we then determined the fraction of Plk1-regulated phosphoproteins and the fraction of all proteins (harboring SAM-analyzed phosphosites) in which they were identified. Respective p values were calculated with Fisher's exact test, one-tailed.

Enrichment analysis in the Gene Ontology (GO) cellular component or molecular function categories was performed for Plk1-up-regulated phosphoproteins (according to SAM analysis at an FDR of 0%, 372 IPI entries) compared with either all phosphoproteins with quantified phosphorylation changes from Plk1^{as} cells (4463 IPI entries) or the entire IPI database by nonconditional hypergeometric testing using the GO stats package (26) in the R statistical environment (21).

For network visualization, all of the identified phosphoproteins with quantified phosphorylation changes that were annotated with the GO cellular component terms centrosome, kinetochore, microtubule, and nuclear pore were submitted to the web-based Search Tool for the Retrieval of Interacting Genes/Proteins (STRING) version 8 (27). Prior to retrieving protein-protein interactions according to the prediction methods "experiments" and "databases," all of the IPI identifiers were converted to Ensembl gene identifiers using the BioMart web server (28). In cases where no Ensembl gene identifier could be assigned, the protein names were subjected to STRING. Only interactions of high confidence (score > 0.7) were considered, and the resulting network was visualized using the Cytoscape software (29).

Accession Information—All of the MS raw data files from this study are accessible in the public repository Tranche (https://tranche.proteomecommons.org/ UTfcT4NzLE9ZabJ6yyjec2i31TXxD9fi2Q/xr-gl4N376GX14liawiTH0oTdZDVU5ufJ9eKZ10kOMGCWOOkxI0IL7ot-QAAAAAAABZJA== for Plk1^{as} cell experiments; N7bS1Xc881fzUd-
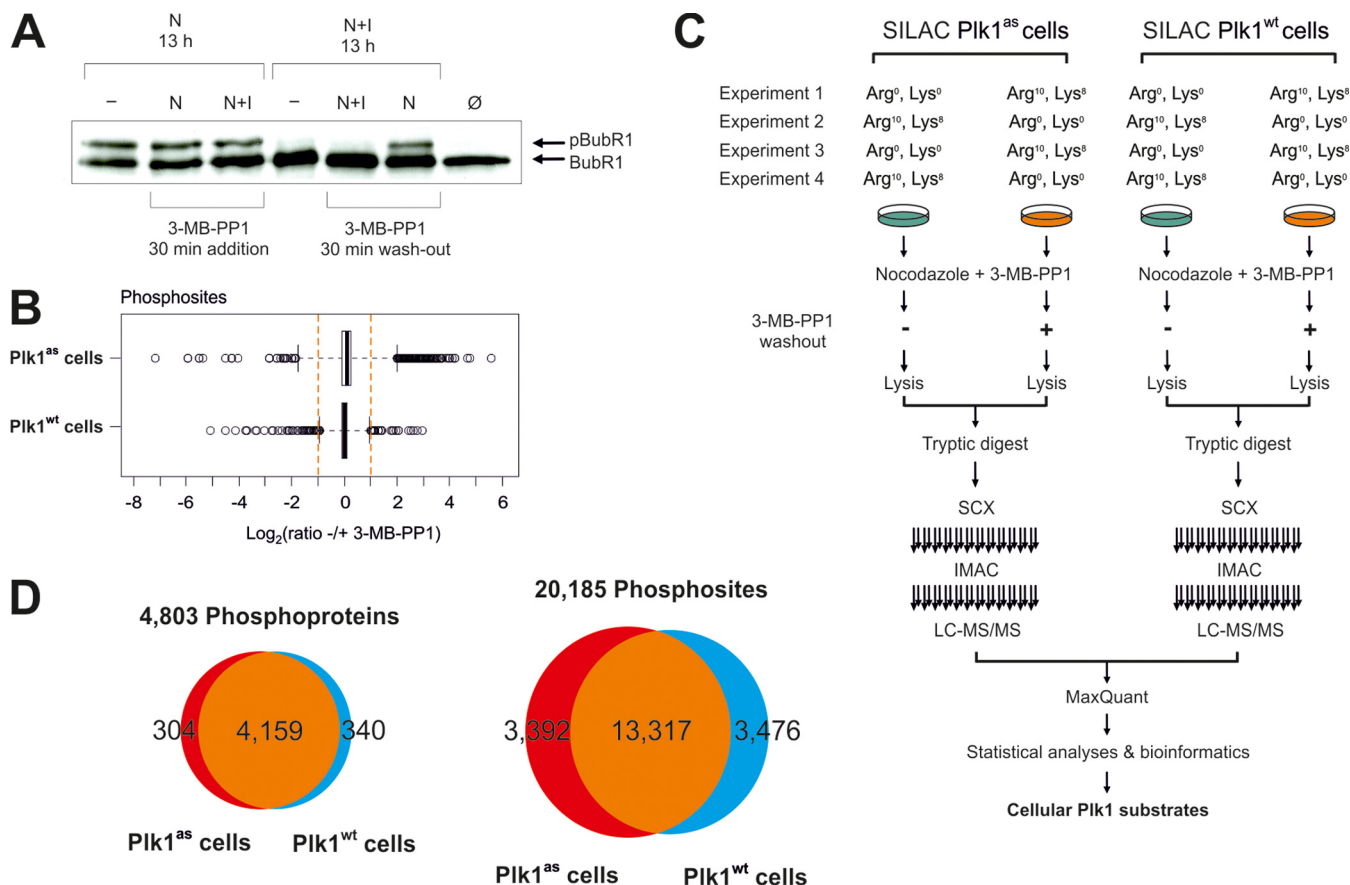
FIG. 1. **Combined chemical genetics and phosphoproteomics approach to identify cellular downstream targets of protein kinases.** *A*, cellular induction of Plk1 activity. Plk1^{as} cells were synchronized and then arrested in mitosis by either nocodazole treatment (*N*) or nocodazole plus 5 μM 3-MB-PP1 inhibitor treatment (*N+I*) for 13 h. The cells were then lysed (—) or washed and incubated for a further 30 min in the presence of either nocodazole (*N*) or nocodazole and 3-MB-PP1 (*N+I*) before lysis. In addition, lysate from nonsynchronized cells was prepared (Ø). Total extracts were then analyzed by immunoblotting with BubR1-specific antibody. The slower migrating band in the *second lane* from the *right* indicates the appearance of Plk1-phosphorylated BubR1 upon 30 min of 3-MB-PP1 wash-out. This treatment condition was compared with continued nocodazole and 3-MB-PP1 incubation (*third lane* from the *right*) in all subsequent SILAC MS experiments. *B*, distributions of phosphorylation site ratios measured upon 3-MB-PP1 wash-out in Plk1^{as} and Plk1^{wt} cell phosphoproteomics experiments. *C*, scheme illustrating the overall experimental design and workflow. Four biological replicate experiments were performed in both Plk1^{as} and Plk1^{wt} cells upon SILAC encoding as indicated. In each experiment, 3-MB-PP1 was washed out from one mitotically arrested cell population before lysis and protein digestion. Phosphopeptides were enriched by SCX chromatography combined with IMAC prior to LC-MS analysis and data processing. *D*, comparison of Plk1^{as} and Plk1^{wt} cell experiments with respect to the overall numbers of quantified phosphorylation sites and phosphoproteins.

qBTMCTjoYGat1eFZxXNcpqJ4zWAYeQIzvQogdgDFYAWtH5EPg-j5hSa8cYvvesNl4j3bJcFXUvReh0AAAAAAABR0g== for Plk1^{wt} cell experiments) using hash codes.

Also available are an Excel spreadsheet listing all peptide evidence data acquired in this study (hash code Qo9HqCzJIPi8fZp9C-ZwZWBKSOtjGQN4FxzYJ8NXzXX409OMzH2NB3TF1w216ZM2Loro-Fa9yZqKM9I2yMl93zTte4/R4AAAAAAAADXg==) and annotated phosphopeptide spectra (hash code LbEiloX/l75TvSvGPkgRgYvIfs/tOTOf8gzt8HhtEejl/I6shfW7uyN+Xk6riIsl33dyjL6JXJrxlrm3/g86HW6-m7JgAAAAAAAM5Dg==).

RESULTS AND DISCUSSION

Pharmacological Induction of Cellular Plk1 Activity—To examine Plk1 inhibition in human retinal pigment epithelial (RPE) cells expressing analog-sensitive mutant (Plk1^{as}), we added the bulky purine analog 3-MB-PP1 to nocodazole-arrested mitotic cells similar to the reported strategy used for Cdk1 substrate identification in yeast (7, 14, 25). Plk1^{as} harboring a mutationally enlarged hydrophobic pocket at the ATP-binding site was previously shown to be inhibited by 3-MB-PP1 *in vitro* and *in vivo*, whereas wild-type Plk1 was not affected by the inhibitor (14). However, even 30 min of 3-MB-PP1 treatment did not suppress phosphorylation of the known Plk1 substrate BubR1 (Fig. 1*A*) (30). This was likely due to inefficient dephosphorylation by cellular phosphatases and indicated a conceptual weakness in the experimental design. We therefore conceived a strategy to rapidly induce suppressed Plk1 activity in mitotically synchronized cells and first arrested cells by prolonged nocodazole treatment with the Plk1^{as} inhibitor 3-MB-PP1 added during synchronization. Plk1-medi-

ated BubR1 phosphorylation was suppressed upon this treatment and, importantly, could then be induced when we washed out the inhibitor as demonstrated by the appearance of the phosphorylated, slower migrating band of BubR1 in Plk1^{as}-expressing cells (Fig. 1*A*). In contrast, 3-MB-PP1 had no effect on BubR1 in control cells expressing wild-type Plk1 (data not shown).

Combination of Chemical Genetics and Quantitative Phosphoproteomics—Next, we performed SILAC of RPE cells expressing either Plk1^{as} or 3-MB-PP1-insensitive wild-type enzyme (Plk1^{wt}) followed by 30 min of inhibitor wash-out from nocodazole-arrested cells to reactivate 3-MB-PP1-inhibited kinases in mitotic cells prior to lysis (1, 18). For quantitative phosphoproteome assessment, we separated proteolytically derived peptides by SCX into 12 fractions prior to phosphopeptide enrichment by IMAC. We performed technical replicate analyses of all IMAC samples by LC-MS on a LTQ-Orbitrap (1, 18). Raw data files were processed with the MaxQuant software for peptide and protein identification and the quantification of phosphorylation changes (4). Finally, phosphorylation site ratios measured in both technical replicate experiments were averaged prior to further data analysis.

By applying this workflow, we identified and quantified ~9,000 distinct phosphorylation sites in either cell line that could be assigned to a specific serine, threonine, or tyrosine residue with a localization probability of at least 0.75 (class I sites) (18). Only class I phosphorylation sites were considered for further analysis throughout this study. Notably, although SILAC quantification reported for 482 sites at least 2-fold changes upon 3-MB-PP1 removal in Plk1^{as} cells, we also recorded as many as 75 such apparent regulations in cells expressing 3-MB-PP1-insensitive Plk1^{wt} (Fig. 1*B* and supplemental Table 1). Because the two cell lines were identical apart from either Plk1^{as} or Plk1^{wt} expression, any phosphorylation changes exclusively recorded in analog-sensitive cells should account for Plk1-mediated phosphorylation events, whereas those occurring in both cell lines would reflect Plk1-independent off-target effects of 3-MB-PP1. The latter could not be excluded because related purine analogs such as NM-PP1 and NA-PP1 were found to inhibit nonmutated protein kinases *in vitro* despite being designed as specific antagonist of mutationally sensitized kinase variants (8). However, the vast majority of sites quantified with greater than 2-fold changes in the Plk1^{wt} cells did not exhibit similar regulation in Plk1^{as} cells upon 3-MB-PP1 wash-out (supplemental Table 1). Of the 46 sites that we quantified with greater than 2-fold changes in Plk1^{wt} cells and that we also quantified in the parallel Plk1^{as} cell analysis, only four exhibited more than 2-fold change in the same direction upon 3-MB-PP1 wash-out from Plk1^{as} cells (supplemental Table 1). Thus, the vast majority of apparent changes in Plk1^{wt} cells most likely reflected the inherent biological and technical variability of the overall experimental workflow. A similar number of such "false positives" in the Plk1^{as} cell analysis would imply that ~15% of

measured changes are not related to cellular Plk1 activity control by 3-MB-PP1, resulting in an estimated FDR we considered as inappropriate.

Evaluation of Biological Replicate Strategy and 3-MB-PP1 Off-Target Identification—Therefore, we extended our analysis to four replicate SILAC analyses per cell line with reversed labeling schemes in consecutive experiments (Fig. 1*C*). In total, we obtained quantitative phosphorylation data for 4803 phosphoproteins and quantified the effect of 3-MB-PP1 wash-out for 20,185 class I sites phosphorylation sites (median localization probability, 0.996) (Fig. 1*D* and supplemental Tables S1 and S2). Our experimental design enabled multiple pair-wise comparisons of independently measured phosphosite ratios across biological replicate analyses (Fig. 2*A*). Almost 3% (on average ~200) of all phosphosites were consistently regulated by more than 2-fold upon 3-MB-PP1 wash-out in the overlap of Plk1^{as} experiments. In contrast, very few phosphosites exhibited reproducible changes in Plk1^{wt} cell comparisons (Fig. 2*A*), and only two of them present on the same doubly phosphorylated peptide were found in consistent ratios across all experiments (supplemental Fig. 1*A*). These sites mapped to casein kinase 1δ (CK1δ) and were also regulated in Plk1^{as} cells (supplemental Fig. 1*A*). Notably, regulation was most likely due to direct cellular CK1δ inhibition, because low micromolar concentrations of 3-MB-PP1 abrogated CK1δ kinase activity *in vitro* (supplemental Fig. 1*B*). However, as these were the sole off-target effects in our large scale analyses, our results indicate high cellular 3-MB-PP1 selectivity against mitotically active protein kinases.

Consequently, our results verified that almost all ratio changes measured in individual Plk1^{wt} cell experiments were due to experimental fluctuations and that two biological replicates dramatically reduced such false positive identifications. Moreover, the number of at least duplicate measurements increased considerably by ~60% when all four instead of just two replicate analyses were considered for Plk1^{as} or Plk1^{wt} cells (Fig. 2*B*).

Statistical Approach to Identify Plk1-regulated Phosphorylations with High Confidence—Our experimental design with parallel biological replicate analyses of Plk1^{as} or Plk1^{wt} cells resulted in a data structure rather similar to gene expression data from microarray measurements, except that SILAC ratios instead of mRNA intensities were measured and missing values were more prevalent in our proteomics data. Building on the similarities, we subjected our data to SAM, which is widely used in transcriptomics and provides FDR estimates based on adjustable thresholds and permutations of replicate data (22).

To identify specific Plk1-mediated phosphorylation events that are differentially induced in Plk1^{as} over Plk1^{wt} control cells upon 3-MB-PP1 wash-out, we restricted our further analysis to the 9204 phosphosite ratios available from at least two biological replicate experiments in both Plk1^{as} and Plk1^{wt}
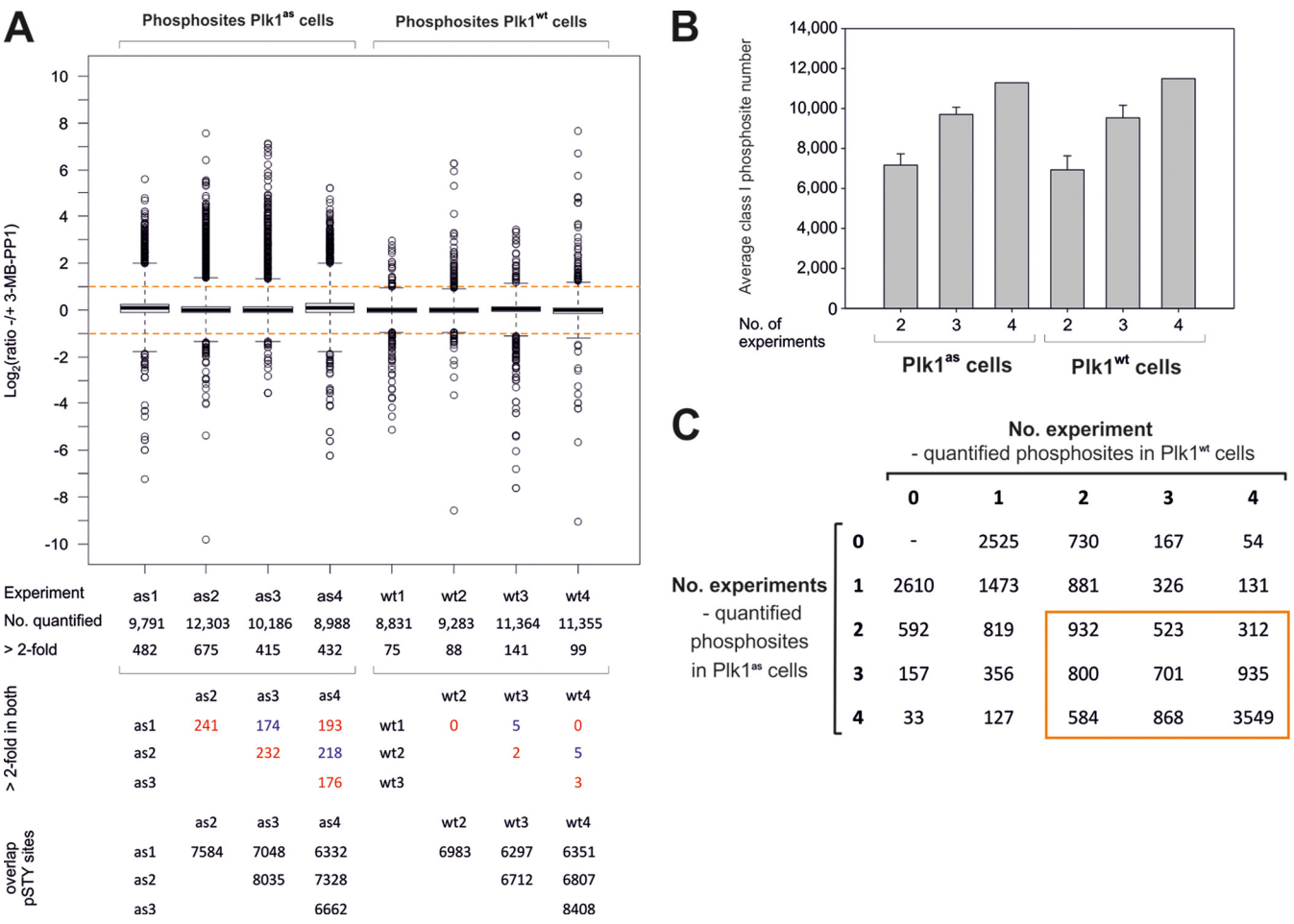
A

Phosphosites Plk1^{as} cells   Phosphosites Plk1^{wt} cells

Log$_2$(ratio -/+ 3-MB-PP1)

Experiment	as1	as2	as3	as4	wt1	wt2	wt3	wt4
No. quantified	9,791	12,303	10,186	8,988	8,831	9,283	11,364	11,355
> 2-fold	482	675	415	432	75	88	141	99

> 2-fold in both

	as2	as3	as4		wt2	wt3	wt4
as1	241	174	193	wt1	0	5	0
as2		232	218	wt2		2	5
as3			176	wt3			3

overlap pSTY sites

	as2	as3	as4		wt2	wt3	wt4
as1	7584	7048	6332		6983	6297	6351
as2		8035	7328			6712	6807
as3			6662				8408

B

Average class I phosphosite number

No. of experiments	2	3	4	2	3	4
		Plk1^{as} cells			Plk1^{wt} cells	

C

No. experiment - quantified phosphosites in Plk1^{wt} cells

		0	1	2	3	4
No. experiments - quantified phosphosites in Plk1^{as} cells	0	-	2525	730	167	54
	1	2610	1473	881	326	131
	2	592	819	932	523	312
	3	157	356	800	701	935
	4	33	127	584	868	3549

FIG. 2. **Evaluation of biological replicate approach for Plk1 downstream target identification.** *A*, ratio distribution and reproducibility across replicate experiments. The distribution of phosphosite ratios for 3-MB-PP1 *versus* control treatment is shown as a *box plot* for all individual Plk1^{as} and Plk1^{wt} biological replicate experiments. For each SILAC analysis, the numbers of all quantified phosphosites and of those measured with more than 2-fold changes upon 3-MB-PP1 wash-out are shown. In the *lower part*, numbers of phosphosites are shown that are more than 2-fold regulated in the same direction (up- or down-regulation) for all pair-wise comparisons of either Plk1^{as} or Plk1^{wt} experiments. In addition, the corresponding numbers of all phosphosites detected in the compared experiments are indicated. *B*, numbers of phosphosites quantified in at least two independent experiments for two, three, and four replicate analyses in either Plk1^{as} or Plk1^{wt} cells. The average numbers determined from all possible combinations of two or three SILAC experiments are shown. *C*, matrix showing the numbers of phosphosites quantified in *x* biological replicate analyses of Plk^{as} and *y* biological replicate analyses Plk^{wt} cells (*x*, *y* = 0, 1, 2, 3, and 4). Phosphosite numbers for all possible combinations are shown. Phosphosites quantified in at least two Plk^{as} and at least two Plk^{wt} cell experiments are boxed.

cells (Fig. 2*C* and supplemental Table 1). Values for missing phosphosite ratios were imputed in the resulting data matrix via a K-nearest neighbor algorithm normalization. SAM retrieved significantly regulated phosphosite subsets along with the corresponding FDRs for different delta (Δ) thresholds (Fig. 3*A*, Table I, and supplemental Table 1). At Δ = 2.136, the 396 most highly ranked phosphosites did not contain any remaining false positive regulation according to SAM (estimated FDR = 0%). Importantly, our experimental data were fully concordant with the statistical analysis, because not a single regulated site according to SAM exhibited stronger 3-MB-PP1-related change in Plk1^{wt} compared with Plk1^{as} cells (Table I and supplemental Table 1). Such apparent behavior would have indicated a false positive identification of a regu-

lated phosphosite, which in this case would have an equal chance to appear more strongly regulated in either cell line, irrespective of Plk1 status. This verified SAM as an adequate tool for stringent statistical analysis that was not compromised by the more frequent missing values in our phosphoproteomics compared with transcriptomics data. Moreover, our results implied apparently error-free identification of phosphoregulation and thus indicated a very high level of confidence. As seen in Fig. 3*B*, as many as 386 of the 396 highly significant changes were due to Plk1^{as} cell-selective up-regulation upon 3-MB-PP1 wash-out and ranged from 1.22-fold to almost 50-fold induction (supplemental Table 1). By contrast, only 10 phosphosites were significantly suppressed upon 3-MB-PP1 wash-out from Plk1^{as} cells, which might
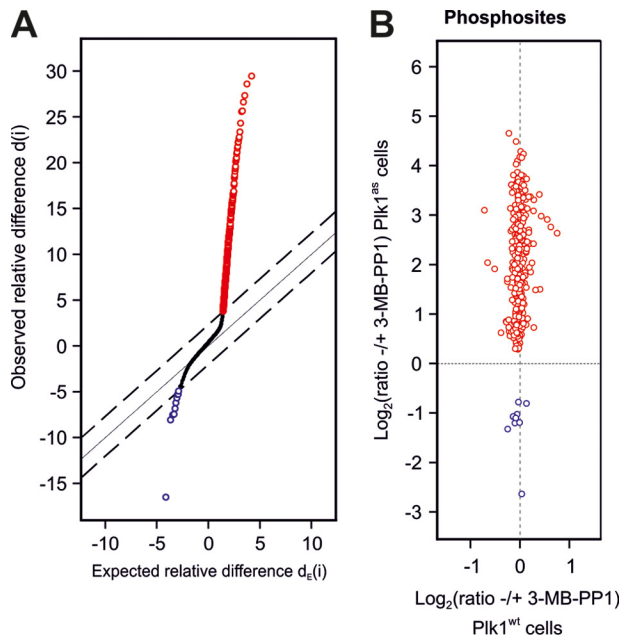
FIG. 3. **Plk1-specific phosphoregulation.** *A*, identification of Plk1-dependent phosphorylation changes by SAM. Shown is a scatter plot of the observed score *versus* the expected score showing the results of differential SAM analysis of Plk1^{as} or Plk1^{wt} ratios. The *solid line* indicates identity of observed and expected scores, whereas the *dashed lines* depict thresholds of $\Delta = 2.136$ beyond which phosphosites were identified as significantly up- and down-regulated (*red and blue circles*) according to an FDR of 0%. *B*, regulated phosphosites with significantly different ±3-MB-PP1 ratios in Plk1^{as} compared with Plk1^{wt} cells. Average ratios from Plk1^{as} cell SILAC analyses were plotted against the respective ratios from Plk1^{wt} experiments. Selectively up- and down-regulated sites in Plk1^{as} *versus* Plk1^{wt} cells are shown as *red and blue circles*, respectively.

be due to Plk1-mediated phosphoregulation of protein phosphatases.

Kinase Substrate Motif Analysis—However, despite short term induction of Plk1 activity, proteins with induced phosphosites were not necessarily direct substrates. To further explore potential kinase-substrate relationships, we extracted sequence motifs that were overrepresented in Plk1-induced sites (24). Plk1 was reported to preferentially phosphorylate sites within an (Asp/Glu/Asn)-Xaa-(Ser(P)/Thr(P))-φ motif, where Xaa represents any amino acid, and φ denotes a hydrophobic residue (25). Notably, all significant motifs either represented the full Plk1 consensus sequence or parts of it (Fig. 4*A* and supplemental Fig. 2). 314 of 386 (81%) of all Plk1-induced sites harbored at least one of the reported specificity determinants in the −2 or +1 position, whereas this was the case for only 28% of all phosphosites that were not significantly regulated (supplemental Table 1). Moreover, this enrichment was even more pronounced when phosphorylation sites in the context of the full Plk1 consensus motif were considered. 38% of all up-regulated phosphosites (148 of 386) matched to the reported Plk1 motif compared with only 2.8% (262 of 8808) of all site-specific phosphorylations that

did not exhibit significant change upon 3-MB-PP1 wash-out (supplemental Table 1). Plk1-regulated phosphoproteins not only exhibited significant enrichment for either Plk1 consensus sites or sites with aspartic acid, glutamic acid, or glutamine in the −2 position, but also for the Ser-(Ser(P)/Thr(P)) motif (Fig. 4*B* and supplemental Table 2), which is recognized by the Plk1 Polo box domain to recruit cellular substrates in a phosphorylation-dependent manner (10, 12). These concordances strongly suggested a large fraction of direct cellular Plk1 modifications detected in our analysis. However, because some protein kinases were found among the Plk1-regulated phosphoproteins (supplemental Table 1), a subset of the observed phosphorylation changes might be mediated through the activation of downstream kinases rather than by direct Plk1 modification.

Cellular Sites of Plk1 Action—Next, we performed GO analysis to validate our data in the context of known Plk1 functions (31). We also included proteins harboring Plk1-regulated phosphopeptides in which phosphoacceptor sites could not be confidently localized in at least two Plk1^{as} and Plk1^{wt} experiments (supplemental Table 3). Using the same criteria as for phosphosites analysis, SAM identified 534 distinct phosphopeptides exhibiting significant regulation Plk1^{as} cells upon 3-MB-PP1 wash-out (supplemental Table 3). In total, our analysis identified 382 distinct proteins as cellular Plk1 downstream targets. We subjected these Plk1-regulated proteins to GO term enrichment analysis using the cellular component annotations of all quantified phosphoproteins from Plk1^{as} cells as reference data (supplemental Table 4). Generally, we found Plk1-regulated phosphoproteins significantly enriched in cellular components such as the centrosome, kinetochore, or spindle apparatus in accordance with known mitotic sites of Plk1 action (Fig. 5*A*) (9). Downstream targets of Plk1 were also prominent among constituents of the nuclear pore, which has recently been appreciated as a major cellular site of Plk1-mediated phosphoregulation (13). Notably, we found Plk1 regulation for 7–29% and identified phosphopeptides for 42–74% of all proteins annotated to the above mentioned and other cellular components enriched for Plk1-regulated phosphoproteins (supplemental Fig. 3*A*). In line with such extensive regulation and high proteome coverage, network analysis revealed Plk1-mediated regulation at multiple nodes within interconnected phosphoprotein networks, thus indicating coordinated control of mitotic processes instead of targeted perturbation of individual components (supplemental Fig. 3*B* and supplemental Table 5).

Plk1-regulated Phosphoproteins—To refine our data analysis to the level of site-specific modifications, we then screened our results for reported *in vivo* and *in vitro* phosphorylation sites of Plk1. Overall, 45 of the 386 up-regulated phosphosites upon cellular Plk1 activation had been described previously, indicating that our experimental approach faithfully recapitulates known mechanisms of cellular Plk1 signaling (supplemental Table 1). Among these 45 sites, 36

TABLE I

Comparison of SAM phosphosite output and experimental data

	SAM output of differential phosphoregulation			Experimental data[a]	
Δ	No. called significant	No. falsely significant	FDR (SAM)	No. regulated in Plk1[as] cells	No. regulated in Plk1[wt] cells
2.136	396	0.0	0.0%	396	0
2.011	406	0.8	0.2%	406	0
1.810	442	0.8	0.2%	442	0
1.609	473	2.3	0.5%	472	1
1.407	509	3.9	0.8%	508	1
1.206	576	8.5	1.5%	575	1
1.005	635	17.8	2.8%	631	4
0.804	784	44.1	5.6%	767	13
0.603	1214	159.5	13.1%	1152	54
0.402	2765	943.0	34.1%	2432	288

[a] For different Δ parameters, all phosphosites for which SAM reported significantly different ratios upon 3-MB-PP1 wash-out in Plk1[as] or in Plk1[wt] cells were analyzed whether their ratios deviated either in Plk1[as] or in Plk1[wt] cells more strongly from one.
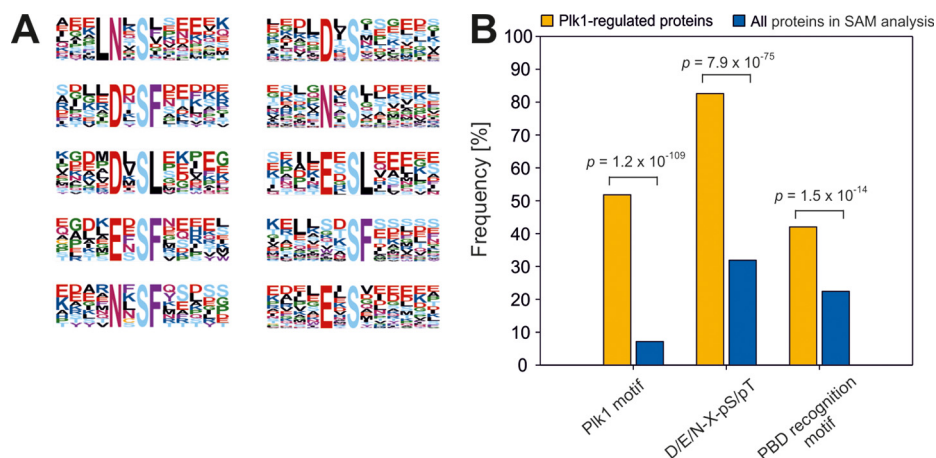

FIG. 4. **Enriched sequence motifs in Plk1-induced phosphorylation sites.** *A*, phosphorylation motifs were extracted with the Motif-X algorithm (24) using all class I serine phosphorylation sites significantly up-regulated upon cellular Plk1 activation. Additional information is provided in supplemental Fig. 2. *B*, frequencies of the Plk1 consensus motif (D/E/N)X(pS/pT)-φ, where X represents any amino acid, and φ denotes a hydrophobic residue (25), its reduced version (D/E/N)X(pS/pT) without a hydrophobic residue in +1 position, and the Polo box domain recognition motif S(pS/pT)(P/X) motif in all proteins with induced phosphosites upon Plk1 activation compared with all phosphoproteins in our SAM analysis.

were reported as down-regulated upon either small molecule or small hairpin RNA inhibition of Plk1 in a recent proteomics analysis of human spindle proteins (13) (supplemental Table 1). In addition to characterized *in vivo* Plk1 sites on mitotic proteins such as Ser[436] of CEP55, Ser[4] of nucleophosmin, or Ser[194] of FADD, our data confirmed cellular regulation of reported *in vitro* Plk1 phosphorylation sites, such as Ser[404] of NEDD1 and Ser[164] of HsCYK-4/MgcRacGAP, as well as of various residues of the anaphase-promoting-complex components APC1, Cdc16, and Cdc27 (Table II). Moreover, because almost 90% of the Plk1-regulated phosphosites found in our current study have not been reported previously, our data provide a vastly extended resource for further functional studies on Plk1-controlled mitotic progression. These studies might include the investigation of new site-specific phosphorylation events on both known and unreported Plk1 substrates localizing to major mitotic compartments, including proteins as diverse as DNA topoisomerase 2α, BubR1, nuclear mitotic apparatus protein 1, RanBP2, and stathmin (Table II). We also

found prominent induction of Cdc25C phosphorylation on Ser[191]. Phosphorylation at this site has been characterized as a modification by the related kinase Plk3, promoting nuclear localization of the Cdc25C phosphatase (32). By extension, our finding suggests an additional mechanism by which Plk1 triggers G$_2$/M transition through Cdc25C regulation. Plk1-mediated phosphoregulation of protein phosphatases might explain the suppression we observed for a few phosphosites in our study upon 3-MB-PP1 wash-out from Plk1[as] cells.

Notably, our results point to possible Plk1 effects on protein ubiquitination beyond the aforementioned regulation of APC components. Cellular Plk1 activation induced site-specific phosphorylations on the E3 ligase HUWE1 and on two components of the SCF (Skp1-Cul1-F-box) ubiquitin ligase complex, SUGT1 and FBXO30. We also identified the ubiquitin carboxyl-terminal hydrolases USP5 and USP47 as cellular Plk1 targets, suggesting coordinated regulation of both ubiquitylation and deubiquitylation during mitotic progression (Table II). To further characterize Plk1-regulated proteins, we
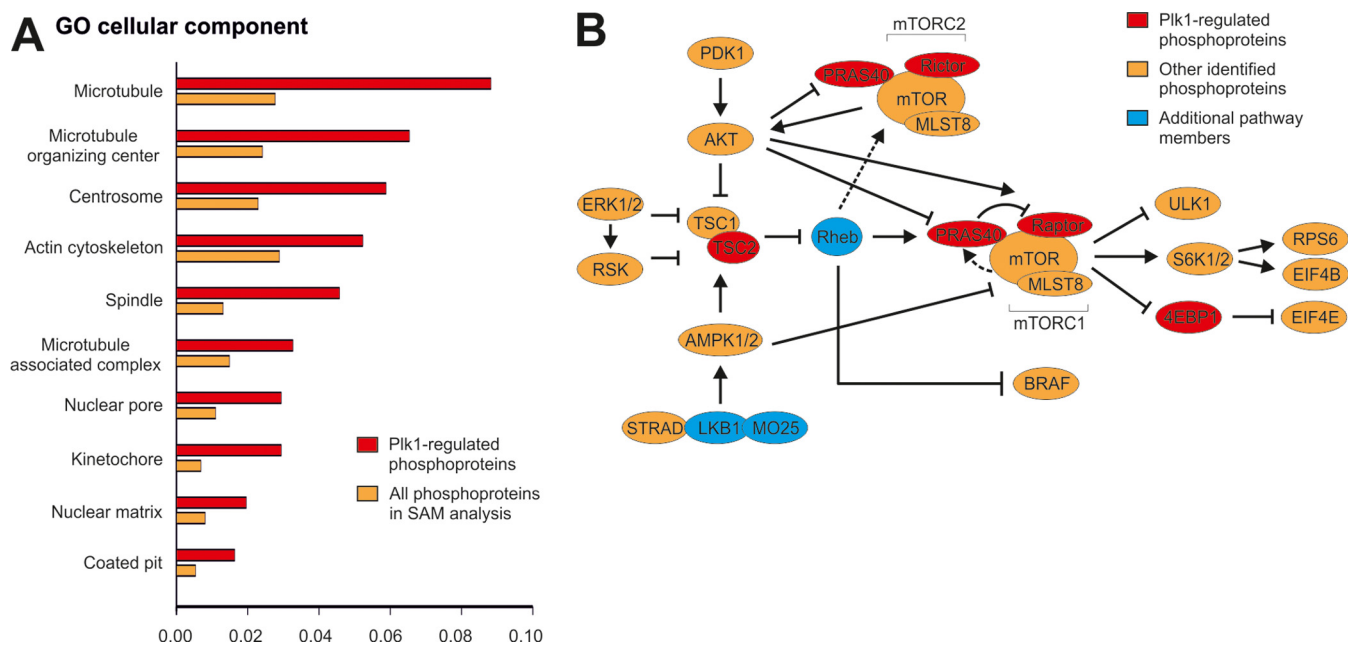
FIG. 5. **Plk1 regulation in cellular compartments and mTOR signaling.** *A*, cellular localization of Plk1-regulated phosphoproteins. Selected GO cellular component terms are shown that were significantly over-represented for Plk1-regulated phosphoproteins compared with all proteins quantified in Plk1^{as} cells ($p < 0.05$). A full list of all GO terms, as well as their enrichment compared with all entries in the human IPI database, is provided in supplemental Table 4. The ratios represent the numbers of proteins with the indicated GO annotation divided by the number of all GO annotated proteins in the respective categories. *B*, Plk1 regulation of the mTOR pathway. Components of the mTOR reference pathway (from the Kyoto Encyclopedia of Genes and Genomes) are shown with Plk1-regulated proteins highlighted in *red*, all other identified phosphoproteins depicted in *orange*, and additional pathway members in *blue*. PRAS40 has been further added based on literature evidence (40).

performed GO enrichment analyses on the level of molecular function. Remarkably, enzymes with helicase activity emerged as a prominent class of Plk1 targets (supplemental Table 6). We identified several Plk1-dependent modification sites on PICH, a Plk1-interacting SNF2 family ATPase implicated in spindle checkpoint signaling (33). Our identification of various other regulated phosphorylations on proteins with ATP-dependent DNA helicase activity points to a rather prominent theme in Plk1 signaling that has been largely unappreciated in previous studies (Table II).

We further analyzed our data for Plk1-regulated phosphoproteins with known functions in signal transduction processes. This revealed several transducers in mammalian target of rapamycin (mTOR) signaling, a signal transduction pathway whose functional role in mitotic progression is still poorly understood (Fig. 5*B* and supplemental Tables 1 and 3) (34). Notably, tuberin underwent phosphoregulation at a Plk1 consensus motif, which points to this previously described Plk1 interactor as a direct substrate (35). Plk1 activation further induced cellular phosphorylation of various other mTOR signaling proteins, including site-specific modifications on rictor, proline-rich Akt substrate 40 kDa, and 4E binding protein 1 (Table II). Moreover, we detected pronounced epidermal growth factor receptor (EGFR) phosphorylation at the Plk1 consensus site Ser^{1064}. This new signaling link might underlie the reported negative regulation of EGFR tyrosine kinase ac-

tivity in mitosis (36). Plk1-mediated EGFR regulation might be part of a concerted mechanism because we recorded elevated phosphorylation on Eps15 and Eps15R, known EGFR substrates with negative regulatory functions in EGFR signaling (37). Eps15 and Eps15R are involved in clathrin-mediated endocytosis, similar to the inositol 5-phosphatase synaptojanin-1, for which we detected enhanced phosphorylation at the Plk1 consensus site Ser^{830} (38). We discovered Plk1-mediated phosphoregulation of several other proteins with distinct enzymatic activities such as the phosphatidylinositol kinase PIK3C2A, poly[ADP-ribose] polymerase 4, DNA (cytosine-5)-methyltransferase 1, and poly(A)-specific ribonuclease PARN (Table II), the latter suggesting a potential mechanism for mRNA stability control during mitotic progression (39).

Collectively, our data point to Plk1 as a cellular regulator of numerous proteins, including many that have not yet been assigned to key mitotic processes. We identified more than 300 Plk1-regulated phosphoproteins in addition to those listed in Table II, and all information about significantly and reproducibly Plk1-regulated phosphosites and phosphopeptides can be accessed in the supplemental data (supplemental Tables 1 and 3). Thus, our data may serve as a valuable resource of numerous new starting points for research in kinase-controlled mitotic progression.

More generally, our integrated chemical genetics and phosphoproteomics approach introduces the concepts of cellular

TABLE II
Selected Plk1-regulated phosphorylation sites

Protein	Short name[a]	Site	Sequence[b]	Plk1[as] Average ratio[c]	Plk1[as] No. ratios[d]	Plk1[wt] Average ratio[c]	Plk1[wt] No. ratios[d]
Centrosomal protein of 55 kDa	CEP55	Ser[436e]	TAALNE**S**LVECPK	7.72	4	0.94	4
Nucleophosmin	NPM1	Ser[4f]	MED**S**MDMDMS	2.41	4	0.98	4
FAS-associated death domain protein	FADD	Ser[194g]	NRSGAM**S**PMSWNS	12.88	2	0.90	2
Rac GTPase-activating protein 1	MgcRacGAP	Ser[154]	ESGSILSDI**S**FDK	10.39	3	0.94	2
Rac GTPase-activating protein 1	MgcRacGAP	Ser[157h]	SILS**DIS**FDKTDE	11.83	3	0.99	2
Rac GTPase-activating protein 1	MgcRacGAP	Ser[170h]	SLDW**DSS**LVKTFK	3.89	3	0.74	3
Protein NEDD1	NEDD1	Ser[404i]	KNQDFS**S**FDDTGK	1.79	3	0.99	4
Anaphase-promoting complex subunit 1	APC1	Ser[377j]	ISSHNQ**S**PKRHSI	5.75	4	0.99	4
Cell division cycle protein 16 homolog	Cdc16	Ser[112j]	KYLK**DES**GFKDPS	20.19	2	1.03	4
Cell division cycle protein 27 homolog	Cdc27	Ser[426j]	QPNIND**S**LEITKL	18.06	4	0.98	4
Cell division cycle protein 27 homolog	Cdc27	Ser[435j]	ITKL**DSS**IISEGK	9.37	4	0.99	4
Cell division cycle protein 27 homolog	Cdc27	Ser[387]	LFTS**DSS**TTKENS	2.12	4	1.01	3
DNA topoisomerase 2α	TOP2A	Thr[1280]	KIKNEN**T**EGSPQE	5.13	2	1.11	4
Mitotic checkpoint serine/threonine-protein kinase BUB1β	BubR1	Thr[710]	PEKLEL**T**NETSEN	13.62	2	0.83	1
Nuclear mitotic apparatus protein 1	NuMA-1	Ser[1789]	QAPLES**S**LDSLGD	3.97	2	0.92	3
E3 SUMO-protein ligase RanBP2	RanBP2	Ser[2270]	TTGF**NFS**FKSALS	6.93	3	0.94	4
Stathmin	STMN1	Ser[46]	PKKK**DLS**LEEIQK	1.71	4	1.00	4
M-phase inducer phosphatase 3	Cdc25C	Ser[191k]	DQAEE**IS**DELMEF	8.82	2	0.88	2
E3 ubiquitin-protein ligase HUWE1	HUWE1	Ser[1368]	GVVR**DLS**MSEEDQ	4.41	4	1.01	4
Suppressor of G₂ allele of SKP1 homolog	SUGT1	Ser[331]	KRAMNK**S**FMESGG	4.38	2	1.00	3
F-box only protein 30	FBXO30	Ser[213]	IGML**NTS**VPNDMD	6.16	2	0.97	3
Ubiquitin carboxyl-terminal hydrolase 47	USP47	Ser[876]	EAILEE**S**TEKLKS	2.81	2	0.99	4
Ubiquitin carboxyl-terminal hydrolase 5	USP5	Ser[760]	GRSAAD**S**ISESVP	6.23	3	1.93	3
DNA excision repair protein ERCC-6-like	PICH	Ser[810]	GTGSAD**S**IATLPK	5.60	2	0.90	2
DNA excision repair protein ERCC-6-like	PICH	Ser[1000]	HSKTCL**S**WEFSEK	1.86	2	0.94	2
DNA excision repair protein ERCC-6-like	PICH	Ser[1004]	CLSWE**FS**EKDDEP	2.06	2	0.96	2
ATP-dependent DNA helicase 2 subunit 1	Ku70	Ser[6]	MSGWE**S**YYKTEG	7.38	4	0.96	4
Chromodomain-helicase-DNA-binding protein 4	CHD-4	Ser[1676]	EKVEEK**S**AIDLTP	8.70	3	0.95	4
Chromodomain-helicase-DNA-binding protein 8	CHD-8	Ser[1544]	RVLD**NFS**DIVEGV	2.12	3	0.96	2
ATP-dependent helicase SMARCAD1	SMARCAD1	Ser[146]	RRND**DIS**ELEDLS	2.06	4	1.00	2
Tuberin	TSC2	Ser[1346]	SSQEEK**S**LHAEEL	2.75	4	1.01	4
Rapamycin-insensitive companion of mTOR	Rictor	Ser[1370]	ITMKAN**S**FESRLT	2.91	4	0.99	4
Proline-rich AKT1 substrate 1	PRAS40	Ser[267]	RPRL**NTS**DFQKLK	4.83	3	0.99	4
Eukaryotic translation initiation factor 4E-binding protein 1	4E-BP1	Ser[112]	RAGGEE**S**QFEMDI	2.98	3	0.97	3
Epidermal growth factor receptor	EGFR	Ser[1064]	CPIKE**DS**FLQRYS	5.65	2	1.02	4
Epidermal growth factor receptor substrate 15	EPS15	Ser[467]	TAELEE**S**VESGKA	2.87	2	1.02	2
Epidermal growth factor receptor substrate 15-like 1	EPS15R	Ser[708]	LDPFE**SS**DPFSSS	5.68	2	0.95	3
Synaptojanin-1	SYNJ1	Ser[830]	LDLL**NAS**FQDESK	4.94	3	1.04	3
Phosphatidylinositol-4-phosphate 3-kinase C2 domain-containing α polypeptide	PIK3C2A	Ser[108]	KLLL**DDS**FETKKT	15.33	3	1.02	4
Poly [ADP-ribose] polymerase 4	PARP4	Ser[1288]	EKLL**DLS**WTESCK	7.05	4	0.97	4
Poly [ADP-ribose] polymerase 4	PARP4	Thr[768]	NENLQD**T**VEKICI	2.62	4	1.03	4
DNA (cytosine-5)-methyltransferase 1	DNMT1	Ser[456]	IFDA**NES**GFESYE	10.14	3	0.99	2
Poly(A)-specific ribonuclease PARN	PARN	Ser[557]	HYYR**NNS**FTAPST	2.70	4	1.01	4

[a] Short protein name according to PhosphoSitePlus database (http://www.phosphosite.org).

[b] Phosphorylation sites are highlighted in bold type, and residues in −2 and /or +1 positions are underlined if consistent with Plk1 substrate consensus motif (D/E/N)X(pS/pT)(F/L/I/Y/W/V/M) (25).

[c] Average ± 3-MB-PP1 ratio measured in Plk1[as] and Plk1[wt] cell experiments.

[d] Number of biological replicate experiments in which the phosphosite ratio was quantified.

[e] Reported *in vivo* Plk1 site (41).

[f] Reported *in vivo* Plk1 site (42).

[g] Reported *in vivo* Plk1 site (43).

[h] Reported *in vivo* Plk1 sites (25).

[i] Reported *in vitro* Plk1 site (44); phosphosite position according to entry in IPI database, corresponds to Ser[397] of the UniProtKB entry NEDD1_HUMAN.

[j] Reported *in vitro* Plk1 sites (45).

[k] Reported *in vivo* site for Plk3 (32).

kinase activation, off-target surveillance, and high confidence identification of downstream targets according to stringent FDR filtering. In principle, our experimental set-up can be applied to any protein kinase that can be sensitized or desensitized to small molecule inhibition. We believe these advances will be highly significant for future efforts to delineate kinase-substrate networks in the physiological cellular context. More generally, experimental strategies similar to those described here might be adopted for a wide range of comparative MS studies and enable the identification of even subtle modifications or protein changes with very high confidence.

Conclusions—We have advanced the combination of chemical genetics and large scale, MS-based phosphoproteomics for the systematic identification of cellular downstream targets regulated by a protein kinase. Our refined approach employs inhibitor-sensitive and -resistant kinase variants and introduces three concepts that enabled confident identification of cellular phosphoregulation through the mitotic regulator Plk1. First, Plk1 activity was induced by cellular inhibitor wash-out to directly trace kinase substrate phosphorylation. Second, in addition to analyzing cells expressing Plk1 mutant with engineered sensitivity to a small molecule inhibitor, we performed parallel control experiments with wild-type Plk1 cells for systematic surveillance of inhibitor off-target effects. Third, we undertook independent replicate analyses of cells harboring wild-type and inhibitor-sensitive Plk1. This enabled highly confident identification of regulated phosphorylation sites on Plk1 downstream targets, which we could verify by full concordance of statistical and experimental data. Our analysis unveiled Plk1-regulated phosphorylations on more than 300 distinct proteins and points to a number of uncharacterized aspects of Plk1-controlled mitotic progression. Most of these have not been reported previously. Therefore our data provide a vastly extended resource for further studies of cellular Plk1 function. Because our experimental strategies can be adopted for any protein kinase amenable to small molecule sensitization or desensitization, the concepts introduced in this study should be of general utility for the systematic and confident identification of cellular kinase-substrate relationships.

Ⓢ This article contains supplemental material.

§ These authors contributed equally to this work.

REFERENCES

1. Dephoure, N., Zhou, C., Villén, J., Beausoleil, S. A., Bakalarski, C. E., Elledge, S. J., and Gygi, S. P. (2008) A quantitative atlas of mitotic phosphorylation. *Proc. Natl. Acad. Sci. U.S.A.* **105,** 10762–10767

2. Olsen, J. V., de Godoy, L. M., Li, G., Macek, B., Mortensen, P., Pesch, R., Makarov, A., Lange, O., Horning, S., and Mann, M. (2005) Parts per million mass accuracy on an Orbitrap mass spectrometer via lock mass injection into a C-trap. *Mol. Cell. Proteomics* **4,** 2010–2021

3. Schreiber, T. B., Mäusbacher, N., Breitkopf, S. B., Grundner-Culemann, K., and Daub, H. (2008) Quantitative phosphoproteomics: An emerging key technology in signal-transduction research. *Proteomics* **8,** 4416–4432

4. Cox, J., and Mann, M. (2008) MaxQuant enables high peptide identification rates, individualized p.p.b.-range mass accuracies and proteome-wide protein quantification. *Nat. Biotechnol.* **26,** 1367–1372

5. Tan, C. S., and Linding, R. (2009) Experimental and computational tools useful for (re)construction of dynamic kinase-substrate networks. *Proteomics* **9,** 5233–5242

6. Bishop, A. C., Ubersax, J. A., Petsch, D. T., Matheos, D. P., Gray, N. S., Blethrow, J., Shimizu, E., Tsien, J. Z., Schultz, P. G., Rose, M. D., Wood, J. L., Morgan, D. O., and Shokat, K. M. (2000) A chemical switch for inhibitor-sensitive alleles of any protein kinase. *Nature* **407,** 395–401

7. Holt, L. J., Tuch, B. B., Villén, J., Johnson, A. D., Gygi, S. P., and Morgan, D. O. (2009) Global analysis of Cdk1 substrate phosphorylation sites provides insights into evolution. *Science* **325,** 1682–1686

8. Bain, J., Plater, L., Elliott, M., Shpiro, N., Hastie, C. J., McLauchlan, H., Klevernic, I., Arthur, J. S., Alessi, D. R., and Cohen, P. (2007) The selectivity of protein kinase inhibitors: A further update. *Biochem. J.* **408,** 297–315

9. Archambault, V., and Glover, D. M. (2009) Polo-like kinases: Conservation and divergence in their functions and regulation. *Nat. Rev. Mol. Cell Biol.* **10,** 265–275

10. Elia, A. E., Cantley, L. C., and Yaffe, M. B. (2003) Proteomic screen finds pSer/pThr-binding domain localizing Plk1 to mitotic substrates. *Science* **299,** 1228–1231

11. Snead, J. L., Sullivan, M., Lowery, D. M., Cohen, M. S., Zhang, C., Randle, D. H., Taunton, J., Yaffe, M. B., Morgan, D. O., and Shokat, K. M. (2007) A coupled chemical-genetic and bioinformatic approach to Polo-like kinase pathway exploration. *Chem. Biol.* **14,** 1261–1272

12. Lowery, D. M., Clauser, K. R., Hjerrild, M., Lim, D., Alexander, J., Kishi, K., Ong, S. E., Gammeltoft, S., Carr, S. A., and Yaffe, M. B. (2007) Proteomic screen defines the Polo-box domain interactome and identifies Rock2 as a Plk1 substrate. *EMBO J.* **26,** 2262–2273

13. Santamaria, A., Wang, B., Elowe, S., Malik, R., Zhang, F., Bauer, M., Schmidt, A., Silljé, H. H., Körner, R., and Nigg, E. A. (2010) The Plk1-dependent phosphoproteome of the early mitotic spindle. *Mol. Cell. Proteomics* **10,** 10.1074/M110.004457

14. Burkard, M. E., Randall, C. L., Larochelle, S., Zhang, C., Shokat, K. M., Fisher, R. P., and Jallepalli, P. V. (2007) Chemical genetics reveals the requirement for Polo-like kinase 1 activity in positioning RhoA and triggering cytokinesis in human cells. *Proc. Natl. Acad. Sci. U.S.A.* **104,** 4383–4388

15. Daub, H., Olsen, J. V., Bairlein, M., Gnad, F., Oppermann, F. S., Körner, R., Greff, Z., Kéri, G., Stemmann, O., and Mann, M. (2008) Kinase-selective enrichment enables quantitative phosphoproteomics of the kinome across the cell cycle. *Mol. Cell* **31,** 438–448

16. Villén, J., and Gygi, S. P. (2008) The SCX/IMAC enrichment approach for global phosphorylation analysis by mass spectrometry. *Nat. Protoc.* **3,** 1630–1638

17. Rappsilber, J., Mann, M., and Ishihama, Y. (2007) Protocol for micro-purification, enrichment, pre-fractionation and storage of peptides for proteomics using StageTips. *Nat. Protoc.* **2,** 1896–1906

18. Olsen, J. V., Blagoev, B., Gnad, F., Macek, B., Kumar, C., Mortensen, P., and Mann, M. (2006) Global, *in vivo*, and site-specific phosphorylation dynamics in signaling networks. *Cell* **127,** 635–648

19. Schroeder, M. J., Shabanowitz, J., Schwartz, J. C., Hunt, D. F., and Coon, J. J. (2004) A neutral loss activation method for improved phosphopeptide sequence analysis by quadrupole ion trap mass spectrometry. *Anal. Chem.* **76,** 3590–3598

20. Olsen, J. V., Vermeulen, M., Santamaria, A., Kumar, C., Miller, M. L., Jensen, L. J., Gnad, F., Cox, J., Jensen, T. S., Nigg, E. A., Brunak, S., and Mann, M. (2010) Quantitative phosphoproteomics reveals widespread full phosphorylation site occupancy during mitosis. *Sci. Signal.* **3,** ra3

21. R Development Core Team (2008) *R: A language and environment for statistical computing*, R Foundation for Statistical Computing, Vienna, Austria

22. Tusher, V. G., Tibshirani, R., and Chu, G. (2001) Significance analysis of microarrays applied to the ionizing radiation response. *Proc. Natl. Acad. Sci. U.S.A.* **98,** 5116–5121

23. Sharma, K., Weber, C., Bairlein, M., Greff, Z., Kéri, G., Cox, J., Olsen, J. V., and Daub, H. (2009) Proteomics strategy for quantitative protein interaction profiling in cell extracts. *Nat. Methods* **6,** 741–744

24. Schwartz, D., and Gygi, S. P. (2005) An iterative statistical approach to the identification of protein phosphorylation motifs from large-scale data sets. *Nat. Biotechnol.* **23,** 1391–1398

25. Burkard, M. E., Maciejowski, J., Rodriguez-Bravo, V., Repka, M., Lowery, D. M., Clauser, K. R., Zhang, C., Shokat, K. M., Carr, S. A., Yaffe, M. B., and Jallepalli, P. V. (2009) Plk1 self-organization and priming phosphorylation of HsCYK-4 at the spindle midzone regulate the onset of division in human cells. *PLoS Biol.* **7,** e1000111

26. Falcon, S., and Gentleman, R. (2007) Using GOstats to test gene lists for GO term association. *Bioinformatics* **23,** 257–258

27. Jensen, L. J., Kuhn, M., Stark, M., Chaffron, S., Creevey, C., Muller, J., Doerks, T., Julien, P., Roth, A., Simonovic, M., Bork, P., and von Mering, C. (2009) STRING 8: A global view on proteins and their functional interactions in 630 organisms. *Nucleic Acids Res.* **37,** D412–D416

28. Haider, S., Ballester, B., Smedley, D., Zhang, J., Rice, P., and Kasprzyk, A. (2009) BioMart Central Portal: Unified access to biological data. *Nucleic Acids Res.* **37,** W23–W27

29. Cline, M. S., Smoot, M., Cerami, E., Kuchinsky, A., Landys, N., Workman, C., Christmas, R., Avila-Campilo, I., Creech, M., Gross, B., Hanspers, K., Isserlin, R., Kelley, R., Killcoyne, S., Lotia, S., Maere, S., Morris, J., Ono, K., Pavlovic, V., Pico, A. R., Vailaya, A., Wang, P. L., Adler, A., Conklin, B. R., Hood, L., Kuiper, M., Sander, C., Schmulevich, I., Schwikowski, B., Warner, G. J., Ideker, T., and Bader, G. D. (2007) Integration of biological networks and gene expression data using Cytoscape. *Nat. Protoc.* **2,** 2366–2382

30. Elowe, S., Hümmer, S., Uldschmid, A., Li, X., and Nigg, E. A. (2007) Tension-sensitive Plk1 phosphorylation on BubR1 regulates the stability of kinetochore microtubule interactions. *Genes Dev.* **21,** 2205–2219

31. Ashburner, M., Ball, C. A., Blake, J. A., Botstein, D., Butler, H., Cherry, J. M., Davis, A. P., Dolinski, K., Dwight, S. S., Eppig, J. T., Harris, M. A., Hill, D. P., Issel-Tarver, L., Kasarskis, A., Lewis, S., Matese, J. C., Richardson, J. E., Ringwald, M., Rubin, G. M., and Sherlock, G. (2000) Gene Ontology: Tool for the unification of biology. The Gene Ontology Consortium. *Nat. Genet.* **25,** 25–29

32. Bahassiel, M., Hennigan, R. F., Myer, D. L., and Stambrook, P. J. (2004) Cdc25C phosphorylation on serine 191 by Plk3 promotes its nuclear translocation. *Oncogene* **23,** 2658–2663

33. Baumann, C., Körner, R., Hofmann, K., and Nigg, E. A. (2007) PICH, a centromere-associated SNF2 family ATPase, is regulated by Plk1 and required for the spindle checkpoint. *Cell* **128,** 101–114

34. Wang, X., and Proud, C. G. (2009) Nutrient control of TORC1, a cell-cycle regulator. *Trends Cell Biol.* **19,** 260–267

35. Astrinidis, A., Senapedis, W., Coleman, T. R., and Henske, E. P. (2003) Cell cycle-regulated phosphorylation of hamartin, the product of the tuberous sclerosis complex 1 gene, by cyclin-dependent kinase 1/cyclin B. *J. Biol. Chem.* **278,** 51372–51379

36. Kiyokawa, N., Lee, E. K., Karunagaran, D., Lin, S. Y., and Hung, M. C. (1997) Mitosis-specific negative regulation of epidermal growth factor receptor, triggered by a decrease in ligand binding and dimerization, can be overcome by overexpression of receptor. *J. Biol. Chem.* **272,** 18656–18665

37. Naslavsky, N., and Caplan, S. (2011) EHD proteins: Key conductors of endocytic transport. *Trends Cell Biol.* **21,** 122–131

38. Astle, M. V., Horan, K. A., Ooms, L. M., and Mitchell, C. A. (2007) The inositol polyphosphate 5-phosphatases: traffic controllers, waistline watchers and tumour suppressors? *Biochem. Soc. Symp*. 161–181

39. Ross, J. (1997) A hypothesis to explain why translation inhibitors stabilize mRNAs in mammalian cells: mRNA stability and mitosis. *Bioessays* **19,** 527–529

40. Sancak, Y., Thoreen, C. C., Peterson, T. R., Lindquist, R. A., Kang, S. A., Spooner, E., Carr, S. A., and Sabatini, D. M. (2007) PRAS40 is an insulin-regulated inhibitor of the mTORC1 protein kinase. *Mol. Cell* **25,** 903–915

41. Fabbro, M., Zhou, B. B., Takahashi, M., Sarcevic, B., Lal, P., Graham, M. E., Gabrielli, B. G., Robinson, P. J., Nigg, E. A., Ono, Y., and Khanna, K. K. (2005) Cdk1/Erk2- and Plk1-dependent phosphorylation of a centrosome protein, Cep55, is required for its recruitment to midbody and cytokinesis. *Dev. Cell* **9,** 477–488

42. Zhang, H., Shi, X., Paddon, H., Hampong, M., Dai, W., and Pelech, S. (2004) B23/nucleophosmin serine 4 phosphorylation mediates mitotic functions of polo-like kinase 1. *J. Biol. Chem.* **279,** 35726–35734

43. Alappat, E. C., Feig, C., Boyerinas, B., Volkland, J., Samuels, M., Murmann, A. E., Thorburn, A., Kidd, V. J., Slaughter, C. A., Osborn, S. L., Winoto, A., Tang, W. J., and Peter, M. E. (2005) Phosphorylation of FADD at serine 194 by CKIα regulates its nonapoptotic activities. *Mol. Cell* **19,** 321–332

44. Zhang, X., Chen, Q., Feng, J., Hou, J., Yang, F., Liu, J., Jiang, Q., and Zhang, C. (2009) Sequential phosphorylation of Nedd1 by Cdk1 and Plk1 is required for targeting of the γTuRC to the centrosome. *J. Cell Sci.* **122,** 2240–2251

45. Kraft, C., Herzog, F., Gieffers, C., Mechtler, K., Hagting, A., Pines, J., and Peters, J. M. (2003) Mitotic regulation of the human anaphase-promoting complex by phosphorylation. *EMBO J.* **22,** 6598–6609